Materials
Views
www.MaterialsViews.com

ADVANCED
MATERIALS
www.advmat.de

COMMUNICATION

Digitization of Endocytic pH by Hybrid Ultra-pH-Sensitive Nanoprobes at Single-Organelle Resolution

Yiguang Wang,* Chensu Wang, Yang Li, Gang Huang, Tian Zhao, Xinpeng Ma, Zhaohui Wang, Baran D. Sumer, Michael A. White, and Jinming Gao*

Responsive nanomaterials have rapidly evolved in a variety of optical, electrical, and mechanical systems in a wide range of applications such as biosensing, self-healing, tissue engineering, and drug delivery.[1] Early work by Mirkin and co-workers demonstrated that small changes in input biochemical signals such as DNA concentration can be transduced into remarkably increased optical signals from gold nanoparticles.[2] Compared to single molecular sensors, nanosensors can amplify signals through positive cooperativity arising from noncovalent self-assembly chemistry.[3] Despite successful development of various nanosystems that respond to external stimuli, nanomaterials-based biosensors that can consistently convert subtle differences into a discrete signal without introducing noise are still lacking.

Endosomes, lysosomes, and related catabolic organelles are recognized as the center for signal transduction events that preserve metabolic homeostasis as well as coordinate cell and tissue responses to nutrient availability.[4,5] A recent study reported the correlation between lysosome acidification capacity and mitochondrial health as a key determinant of cellular aging in yeast.[6] Moreover, aberrant regulation of endosome/lysosome functions has been associated with a variety of malignances, such as Alzheimer's disease,[7] lysosome storage disease,[8] and autoimmunity disorder. Despite the physiological importance of endosomes and lysosomes, there is no available method to image the dynamic maturation process of these organelles. Endocytic pH is a hallmark of endosome maturation,

where luminal pH changes continuously from 7.2 (extracellular environment) to lower than 4.5 (lysosomes). Conventional small molecular pH sensors (e.g., LysoTracker) diffuse through lipid membranes and fluoresce upon accumulation and activation inside acidic organelles. These agents are not able to accurately report the maturation process because of the indiscriminate contribution to fluorescence intensity from organelle pH or probe concentration, as well as signal deterioration by photobleaching or nonspecific contributions from other acidic organelles (e.g. Golgi).[4]

Herein we report a hybrid ultra-pH-sensitive (HyUPS) nanotransistor probe to image and quantify the acidification process of endocytic organelles in live cells. Transistors are commonly used as electronic switches because they respond sharply to a voltage threshold with an amplified current output. In this hybrid nanoparticle design, we produced a molecular mixture of three different ultra-pH-sensitive block copolymers each serving as a binary pH threshold sensor at a predetermined pH value (**Figure 1**). Each polymer–dye conjugate exhibits an amplified (>30 fold) and sharp (<0.25 pH) response at its specific transition pH (pH_t). In this study, pH_t values of 6.9, 6.2, and 5.3 were chosen to report their activation at clathrin-coated vesicles (CCV) (pH 6.9–7.2),[9] early endosome (pH 6.0–6.5),[10] and late endosome/lysosome (pH 4.0–5.5).[10,11] Each pH transition is encoded with a unique fluorescent reporter. In the micelle state, hetero- and homo-molecular fluorescence energy transfer (hetero-FRET and homo-FRET, respectively) resulted in dramatic quenching of overall fluorescence.[12] As pH drops, the copolymers are sequentially activated at corresponding pH_t with strong emission of fluorescence. Based on the unique multi-pH sensing capability of HyUPS nanotransistors, we were able to quantify the acidification kinetics in live cells at single-organelle resolution. Enabled by HyUPS, we uncovered that an oncogenic signature of KRAS mutation was able to drastically increase the acidification rates of endosomes using a panel of isogenic lung cancer cell lines and further validated this finding in additional cancer cell lines with different genetic backgrounds.

Initially, we synthesized a series of amphiphilic block copolymers PEG-*b*-PR, where PEG is poly(ethylene glycol) and PR is an ionizable segment (Scheme S1 and Table S1, Supporting Information). Each PEG-*b*-PR copolymer was conjugated with a different fluorophore (PR-Dye is used as abbreviations to describe these polymers below). Three exemplary PEPA-BDY, PDPA-TMR, and PDBA-Cy5 fluorescent polymers were synthesized and characterized in dye conjugation number and efficiency as well as quantum yields (Scheme S1 and Table S2, Supporting Information). Individual PEPA-BDY, PDPA-TMR, or PDBA-Cy5 nanoprobes had pH transitions at 6.9, 6.2, and 5.3, respectively.

Dr. Y. Wang, C. Wang, Y. Li, Dr. G. Huang, Dr. T. Zhao,
Dr. X. Ma, Dr. Z. Wang, Prof. J. Gao
Department of Pharmacology
Simmons Comprehensive Cancer Center
UT Southwestern Medical Center at Dallas
5323 Harry Hines Blvd, Dallas, TX 75390, USA
E-mail: wangyiguang1980@bjmu.edu.cn;
jinming.gao@utsouthwestern.edu
Prof. Y. Wang
Beijing Key Laboratory of Molecular Pharmaceutics
and State Key Laboratory of Natural and Biomimetic Drugs
Peking University
Beijing 100191, China
C. Wang, Prof. M. A. White
Department of Cell Biology
UT Southwestern Medical Center at Dallas
5323 Harry Hines Blvd, Dallas, TX 75390, USA
Prof. B. D. Sumer
Department of Otolaryngology
UT Southwestern Medical Center at Dallas
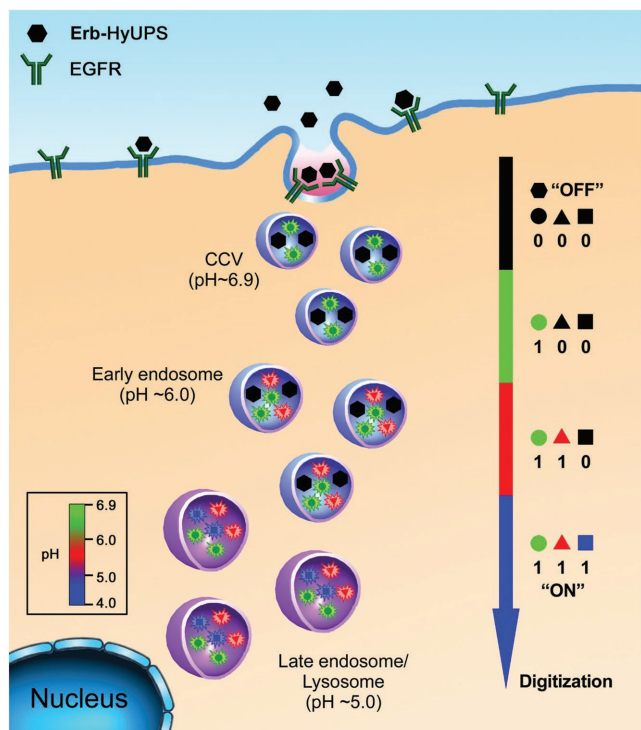5323 Harry Hines Blvd, Dallas, TX 75390, USA

Figure 1. Schematic of the multispectral HyUPS nanoprobe to digitize organelle pH after receptor-mediated endocytosis in tumor cells. The HyUPS nanoprobe stays OFF at pH 7.4. After endocytosis, the PEG-*b*-(PR-*r*-dye) components disassemble and fluoresce sequentially. Three discrete stages of organelle maturation processes can be digitized by a series of barcodes with binary (0 and 1) output in each channel reporting the luminal pH of individual endocytic organelle.

The nanoparticle diameters were 25–35 nm with narrow size distribution. The fluorescent activation ratios (R_F) were 30, 91, and 107 fold for each PEPA-BDY493, PDPA-TMR, and PDBA-Cy5 nanoprobe, respectively, all with sharp pH response ($\Delta pH_{10-90\%} = 0.18-0.22$, Table S3 and Figure S1–S4, Supporting Information). We used the sonication method where the copolymers were first dissolved in THF and then added dropwise into water to produce a molecularly mixed micelle (Supporting Information). The resulting hybrid UPS nanoprobe consists of three components PEPA-BDY, PDPA-TMR, and PDBA-Cy5 in one micelle nanoparticle (Figure 1). We hypothesized that the three fluorescent copolymers will maintain a homogeneous molecular mixture at pH 7.4. After endocytosis, the hybrid UPS nanoprobe will sequentially disassemble and fluoresce at the specific pH_t of each polymer (i.e. 6.9, 6.2, 5.3) to digitize the endosomal maturation process at the single-organelle resolution in living cells (Figure 1).

To demonstrate the formation of a molecularly mixed hybrid nanoparticle, a series of homo-FRET and hetero-FRET experiments was performed. The homo-FRET experiment involves a molecular mixture of one fluorescent PEG-*b*-PR polymer with a different dye-free PEG-*b*-PR polymer. If two copolymers form separate micelles, homo-FRET-induced quenching will cause drastic fluorescence decrease in the dye-conjugated polymer micelles; if the two copolymers form molecularly

mixed micelles, dye separation within the micelle core will not result in significant homo-FRET-induced quenching. In this experiment, we chose PEPA-Cy5 to mix it with dye-free PEPA, PDPA, or PDBA copolymers at the molar ratio of 1:19. Results showed the successful formation of molecularly mixed micelle of PEPA-Cy5 with any of the PEPA, PDPA, or PDBA polymers in the same micelle, which was indicated by the recovery of the Cy5 fluorescent signal (Figure S5, Supporting Information).[13] In contrast, a micelle mixture of PEPA-Cy5 micelle and another label-free micelle at the same molar ratio showed no Cy5 signal recovery. The same result was also observed in the molecularly mixed micelle of PDBA-Cy5 and other label-free PEG-*b*-PR copolymers (Figure S6, Supporting Information).

To further verify the formation of the hybrid nanoprobe, we examined the fluorescence transfer efficiency from copolymers encoded with different hetero-FRET dye pairs: PEPA-BDY, PDPA-TMR, and PDBA-Cy5. To minimize the homo-FRET effect, each copolymer was conjugated with one dye in average in the hydrophobic PR segment. Two or three different copolymers were dissolved in THF and then added dropwise into water to produce a molecularly mixed micelle. In the pair of PEPA-BDY and PDPA-TMR (molar ratio = 1:1), the fluorescence intensity at BDY emission wavelength (i.e., 510 nm) in the molecularly mixed micelle decreased over fourfold as compared to PEPA-BDY alone micelle solution. Moreover, the fluorescence intensity at TMR emission (580 nm) increased over fourfold for molecularly mixed micelle solution over PDPA-TMR micelle solution (Figure S7a, Supporting Information). The other three sets of hetero-FRET polymer pairs: i) PDPA-TMR and PDBA-Cy5, ii) PEPA-BDY and PDBA-Cy5; iii) PEPA-BDY, PDPA-TMR, and PDBA-Cy5 were also investigated (Figure S7, Supporting Information). Interestingly, in the 3-in-1 set, we observed a sequential hetero-FRET effect from BDY to TMR, then to Cy5 (Figure S7d, Supporting Information). The fluorescence intensity at BDY emission in hybrid nanoprobe decreased over fourfold as compared to PEPA-BDY alone micelle solution, while the Cy5 signal increased over 25-fold for hybrid nanoprobe over PDBA-Cy5 alone micelle. These results demonstrate that the PEPA, PDPA, and PDBA copolymers were sufficiently compatible with each other to form a stable homogeneous hybrid nanoparticle.

For biological studies, we finalized a hybrid nanoprobe composition using PEPA-BDY, PDPA-TMR, and PDBA-Cy5 copolymers where each PR chain was conjugated with ≈2.2 dyes (Figure S8, Supporting Information). The fluorescence emission spectra at different excitation wavelengths (i.e., 485, 545, 640 nm) and different pH (i.e., 7.4, 6.7, 5.8, and 5.0) were plotted (**Figure 2**a–d, Figure S10 and S11, Supporting Information). Results show that all three fluorescent polymer modules were "silent" at pH 7.4. When the pH decreased to 6.7, the PEPA-BDY signal was released first to produce the green signal, while the other two modules stayed "OFF." When pH was lowered to 5.8, the PDPA-TMR signal was activated to produce the red signal and the PDBA-Cy5 remained "silent" at this stage. Finally, the PDBA-Cy5 was activated when the solution pH was decreased to 5.0. At this pH, all three fluorescent polymers were fully activated. The particle sizes of hybrid UPS nanoprobes were ≈35 nm at pH between 7.4 and 5.8, and dropped to 8.7 nm as unimers at pH 5.0 as measured by
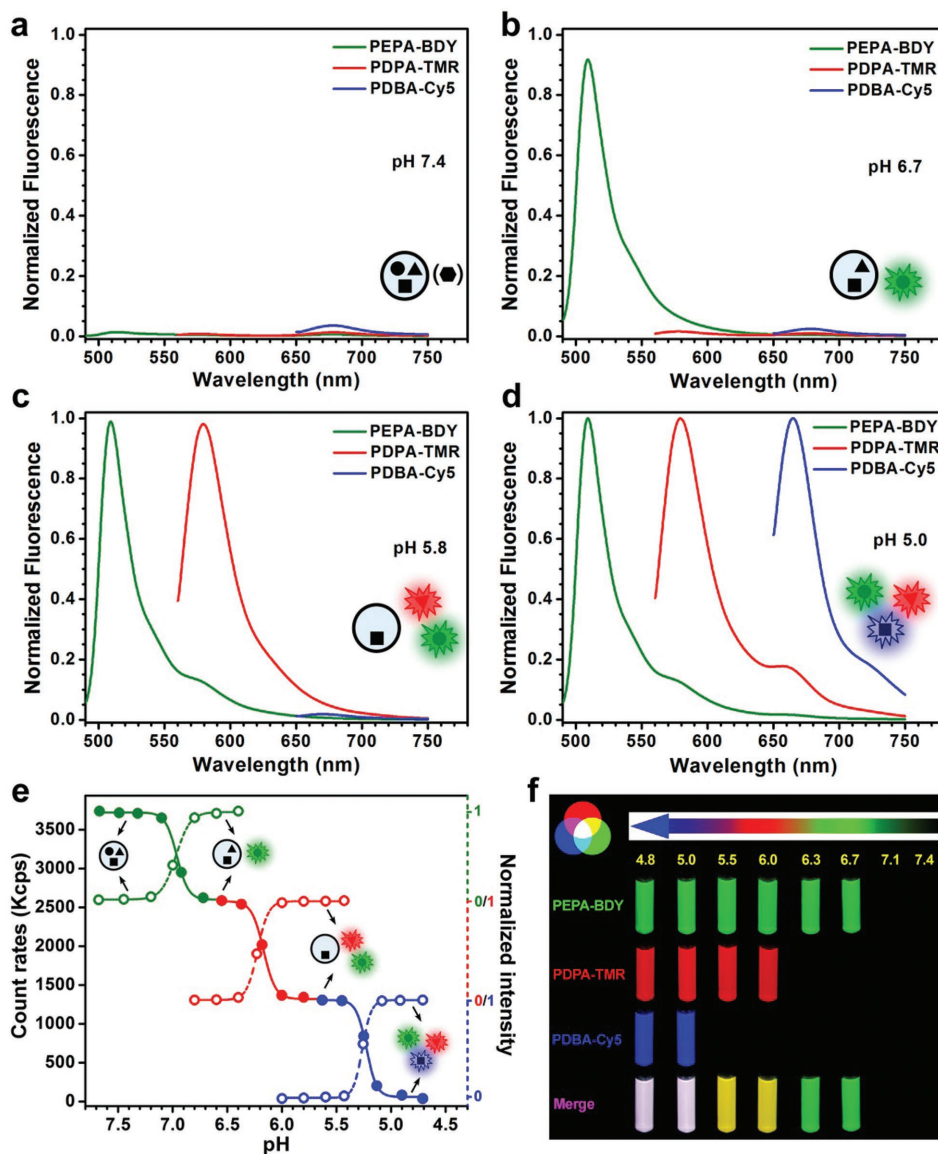
Figure 2. In vitro characterization of the HyUPS nanoprobe. a–d) Fluorescence spectra of the hybrid nanoprobe in different pH buffers. The BDY, TMR, and Cy5 signals were excited at 485, 545, and 640 nm, respectively. e) The count rates and normalized fluorescence intensity of the hybrid nanoprobe are plotted as a function of pH. Multistage activation of the hybrid UPS nanoprobe is shown by green, red, and blue sigmoidal curves at different pH. f) Representative fluorescence images of multispectral HyUPS nanoprobe at different pH. Yellow is the merged color of green and red signals. White is the merged color of blue, green, and red signals.

dynamic light scattering analysis (DLS). Similar observation was made by TEM analysis (Figure S9, Supporting Information). The pH_t values for PEPA-BDY, PDPA-TMR, and PDBA-Cy5 components in hybrid UPS nanoprobe were 6.9, 6.2, and 5.3, which were consistent with corresponding single component nanoprobes. Overall, the fluorescence activation ratios for PEPA-BDY, PDPA-TMR, and PDBA-Cy5 were 74, 123, and 30 with sharp pH responses ($\Delta pH_{10–90\%}$ = 0.20–0.25, Table S4, Supporting Information). The quenching mechanism for each dye was summarized in Table S4 (Supporting Information). The HyUPS nanoprobe is stable for more than one month at 4 °C storage (Table S5, Supporting Information) as demonstrated

by consistent values of pH_t, sharp pH transitions, and fluorescence on/off ratios (Figure S12, Supporting Information). Using DLS analysis, we plotted the count rates of the hybrid nanoprobe versus pH and observed the multistage activation pattern as shown in Figure 2e. At each stage, one fluorescent polymer was found to dissociate, fluoresce, and finally all the polymers dissociated into unimers as indicated by the count rates reaching zero. The multistage activation of the hybrid UPS nanoprobe at different pH values was also imaged and verified by Maestro CRI imaging system as shown in Figure 2f. To evaluate the potential cell toxicity of the hybrid UPS, we performed MTT assay in A549 lung cancer cells. Results showed

ADVANCED
MATERIALS
www.advmat.de

Materials
Views
www.MaterialsViews.com

minimal toxicity (cell viability > 90%) for the HyUPS in the concentration range of 0.1 to 100 µg mL^{-1} (typical imaging dose is below 100 µg mL^{-1}). HyUPS only showed slightly higher toxicity (85% viability) at 1000 µg mL^{-1} (Figure S13, Supporting Information).

To investigate the synchronized cell uptake of all three components in a hybrid UPS nanoprobe, we functionalized the nanoprobe surface with 5% Erbitux (humanized EGFR antibody)[14] Fab'-SH fragment through thiol-maleimide linkage (Supporting Information). The Erb-encoded hybrid nanoprobe had three distinct pH transitions at 6.9, 6.2, and 5.3 with ΔpH$_{10-90\%}$ values of 0.20–0.25. The fluorescence ON/OFF activation ratios of the hybrid nanoprobe were 200, 191, and 35-fold for BDY, TMR, and Cy5 channels, respectively. To investigate the specificity of Erb-encoded UPS nanoprobe, A549 human lung cancer cells were incubated with Erb-encoded PDPA-TMR nanoprobe. Fifteen minutes after Erb-encoded PDPA-TMR incubation, punctate fluorescence activation was observed inside the cells. At 1 h, over 250-fold fluorescence increase in the Erb-encoded PDPA-TMR nanoprobe was observed over Erb-free PDPA-TMR nanoprobe control group, demonstrating EGFR-enhanced endocytosis (Figure S14, Supporting Information). After verifying the specificity of the Erb-conjugated UPS nanoprobe, we checked the synchronized uptake of Erb-encoded hybrid UPS nanoprobe (Figure S15, Supporting Information). A549 cells were incubated with Erb-encoded hybrid UPS nanoprobe for 3 h and imaged by a confocal microscope. In the control group, A549 cells were incubated with a micelle mixture of Erb-free PEPA-BDY micelles, Erb-encoded PDPA-TMR micelles, and Erb-free PDBA-Cy5 micelles. We found all three colors in endocytic organelles from Erb-encoded hybrid nanoprobes, whereas only Erb-encoded PDPA-TMR signal was found in the control group.

To investigate the ability of HyUPS nanoprobe to quantify endosomal maturation, A549 cells were first incubated with Erb-encoded nanoprobes for 30 min at 4 °C to allow for EGFR binding, then the medium was removed and replaced with fresh medium at 37 °C. Intracellular activation of hybrid nanoprobe was imaged by a laser confocal microscope at selected time points. As expected, the PEPA-BDY signal was first released to produce green fluorescent dots at 10 min, and the intensity increased and reached a plateau after 30 min (**Figure 3** and Figure S16, Supporting Information). Red PDPA-TMR signals started to emerge at 20–30 min. All the red dots were co-localized with a subset of green dots at this stage. Finally, the PDBA-Cy5 signal was activated as indicated by pseudocolored blue dots at 90–180 min, and all the blue dots were a subset of red dots in this time period. Based on the sequential activation of HyUPS, we introduced a digital barcode where each digit corresponds to a fluorescent reporter with a binary response (1 for ON, 0 for OFF). The (000) code corresponds to the off state in the cell culture media at pH 7.4. The other three barcodes divide the endocytic pH into three pH-discretized regions: i) green dots (100) that encode a pH threshold between 6.9 and 6.2; ii) yellow dots (110) between 6.2 and 5.3; and iii) white dots (111) for pH below 5.3, which correspond to clathrin-coated vesicles, early endosomes and late endosomes/lysosomes, respectively. We found similar pattern of sequential activation in HN5 head–neck cancer cells (Figure S17, Supporting Information).

Quantitative analyses of distribution of organelles with different digital barcodes illustrate the heterogeneity of organelle maturation (Figure 3b). Over time, a larger population of the endocytic organelles matures from the higher pH vesicles (100) at 30 min to late endosomes/lysosomes (111) at 180 min. The binary output (0 and 1) in each color channel allows a drastically simplified readout of organelle pH compared to small molecular pH sensors (e.g., Lysosensor), where the ratio of continuously changing fluorescence intensity from two different wavelengths needs to be converted to pH values based on a predetermined calibration curve. In addition, photobleaching or background autofluorescence will have a bigger impact on the accuracy of measurement in intensity-based pH measurement by small molecular pH sensors compared to the binary readouts through HyUPS nanoprobes. For example, LysoTracker Red was incubated with A549 cells for lysosome pH sensing and maturation study. Results showed that LysoTracker diffused through lipid membranes and fluoresce upon accumulation and activation inside acidic organelles (Figure S18, Supporting Information). It was not possible to accurately report the maturation process because of the mono-color coding, rapid dye diffusion across membrane lipid, and the indiscriminate contribution to fluorescence intensity from organelle pH or probe concentration.

To track the maturation process of single endocytic organelles in real time, we used HeLa cells that have a faster endosome maturation rate to capture the dynamic process of maturation. Cell images were acquired on a spinning disk confocal microscope equipped with an electron-multiplying charge-coupled device (EMCCD) camera. The images were captured at 1 frame every 15 s with short exposure time. A simplified dual-color HyUPS nanoprobe (PDPA-TMR and PDBA-Cy5) was used in this study. In one example, a relatively stationary organelle as identified by the white arrows in Figure 3c, was monitored over time. We were able to track its maturation based on color change from green (PDPA-TMR positive) to red (PDBA-Cy5 positive) at ≈43 min (Figure 3c and Movie S1, Supporting Information). The time that PDBA-Cy5 punctate signals started to emerge ranged from as early as 20 min to 40 min in different individual organelles revealing stochastic, heterogeneous process of organelle acidification within a single cell. In the meantime, we also observed several fast fusion and fission events (Figure 3c and Movie S1, Supporting Information). A touch-and-separate fusion event between the green dot and red dot was observed at 37 min. A touch-and-separate fusion, i.e., exchange of luminal content while still maintaining two separate vesicles, was noted in various biological studies including endosome–lysosome interactions, exocytosis of neurotransmitters, and autophagosome–lysosome interactions.[15] Interestingly, we observed the red signal activation within the green dot during this event, indicating rapid acidification of endosome following fusion. These results demonstrate the utility of the HyUPS nanoprobe to monitor the dynamic process of organelle maturation at single-organelle resolution.

Next, we investigated the impact of oncogenic signatures on acidification of endocytic organelles. Recent data show that pancreatic cancer cells with KRAS mutations have elevated macropinocytosis rates and lysosomal catabolism of albumins.[16] To investigate whether mutated KRAS also affects acidification rates, we employed a model system consisting of tumor-derived
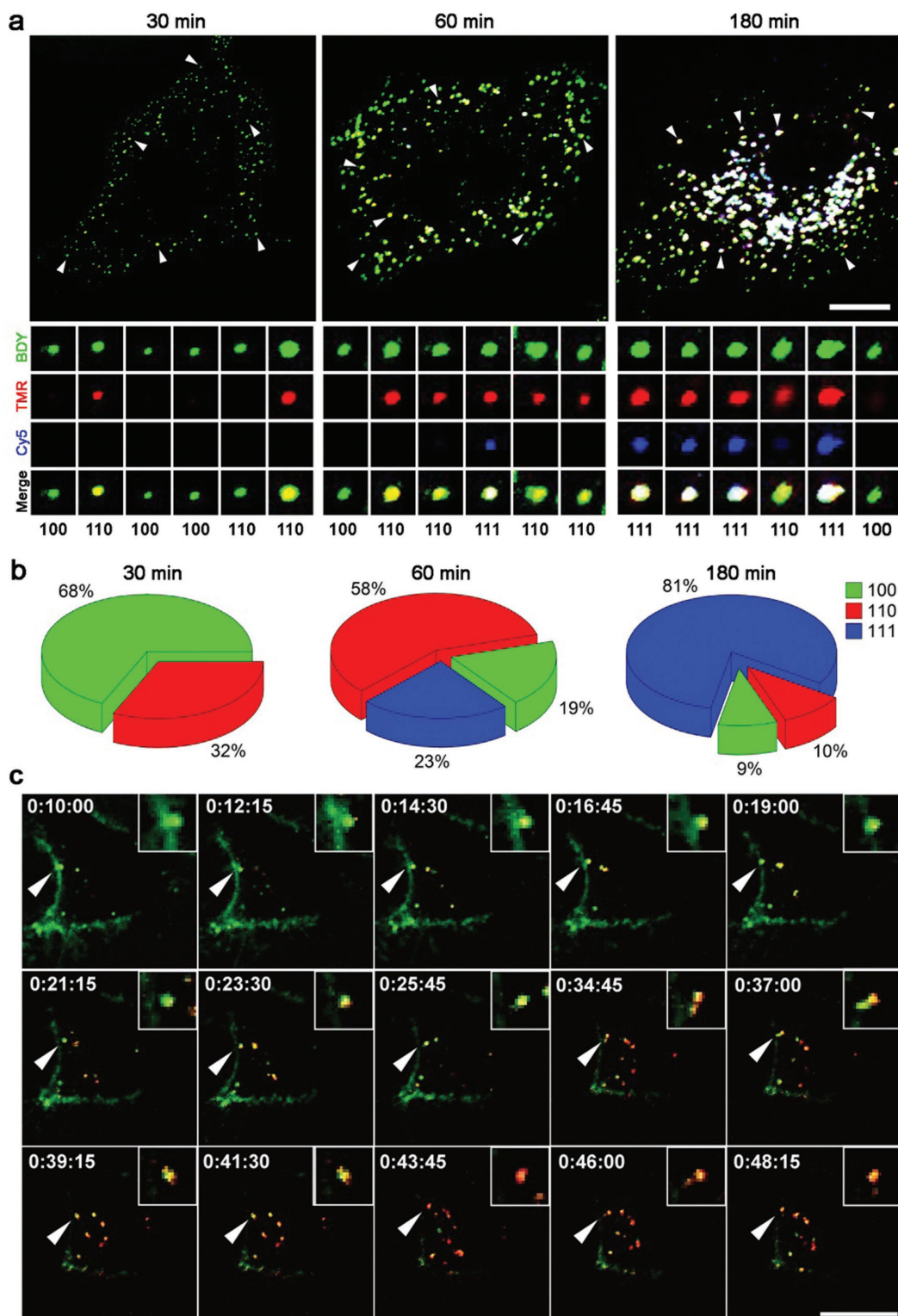
Materials
Views
www.MaterialsViews.com

ADVANCED
MATERIALS
www.advmat.de

Figure 3. Real-time tracking of individual endocytic organelles by HyUPS nanoprobe in live cancer cells. a) pH digitized fluorescent dots at different time showing organelle acidification status. A549 cells were incubated with 100 µg mL^{-1} Erbitux-conjugated HyUPS nanoprobe at 4 °C for 30 min, washed, and imaged in real time at 37 °C by a confocal microscope. BDY, TMR, and Cy5 are shown as green, red, and blue colors, respectively. Six representative pH digitized dots in each cell were enlarged. The scale bar is 10 µm. b) Pie chart showing the distribution of endocytic organelles in different discretized pH regions encoded with specific digital barcodes in live cells. Data were obtained from ten distinct cells. c) Real-time tracking of individual endocytic organelles by the HyUPS nanoprobe. HeLa cells with faster endocytic maturation rates were used in this study on a spin disc confocal microscope. Insets show the zoomed-in images of the organelle pointed by the white arrows. The scale bar is 10 µm. Also see Movie S1 in the Supporting Information.
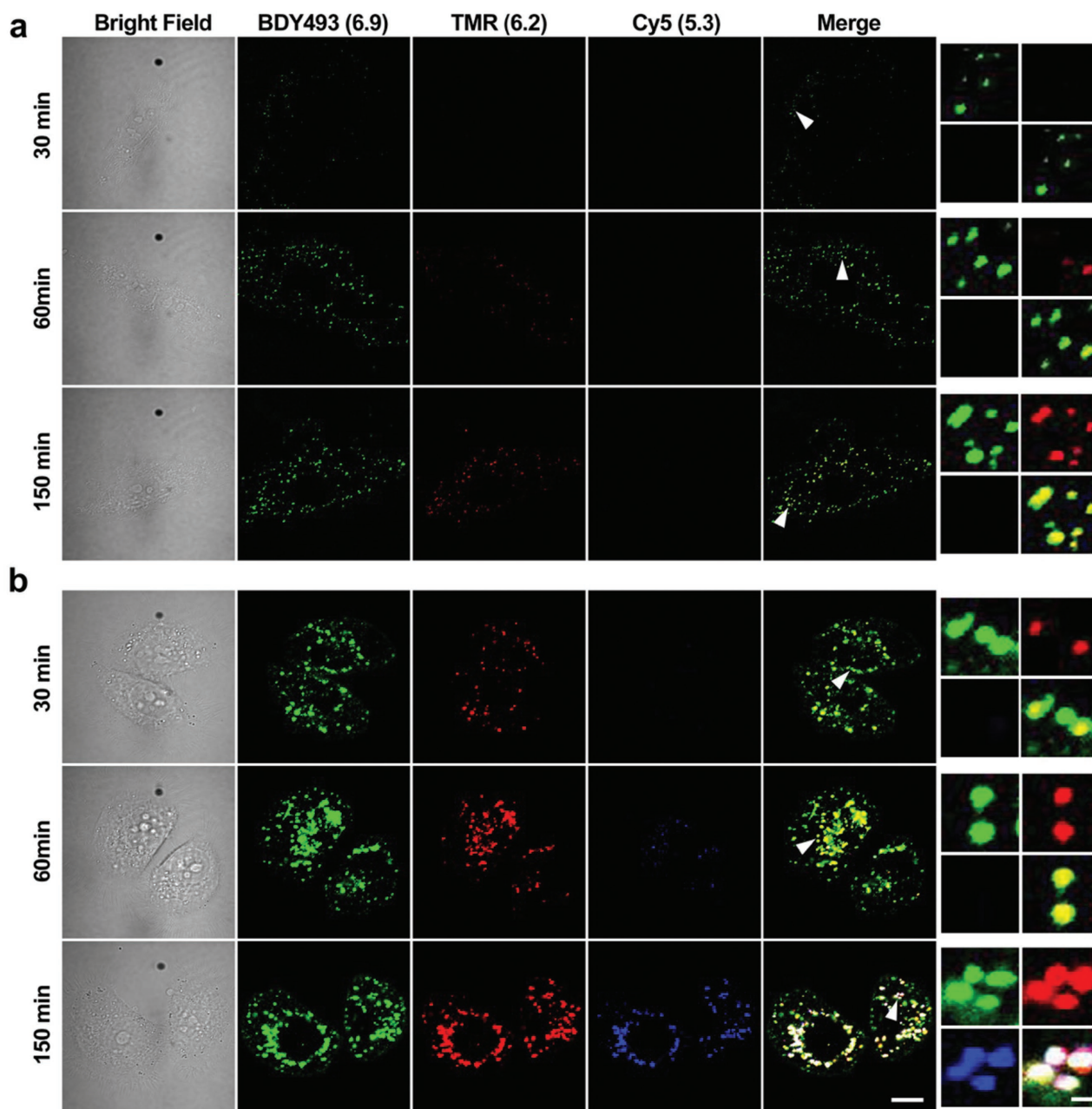
Figure 4. Multistage pH imaging of organelle maturation using multispectral HyUPS nanoprobes in live cells. a) HBEC30KT lung epithelial cells and b) isogenic HCC4017 lung cancer cells were incubated with 100 µg mL^{-1} Erbitux-conjugated HyUPS nanoprobe at 4 °C for 30 min, washed, and imaged in real time at 37 °C by a confocal microscope. BDY, TMR, and Cy5 are shown as green, red, and blue colors, respectively. The scale bar is 10 µm. HyUPS nanoprobes showed dramatically increased acidification rates of endocytic organelles in HCC4017 cells over HBEC30KT cells.

(HCC4017) and normal bronchiole epithelia-derived (HBEC30KT) cell lines from the same lung cancer patient together with an isogenic progression series of HBEC30KT with stepwise stable suppression of TP53 (HBEC30KT-*shTP53*) and KRAS^{G12V} (HBEC30KT-*shTP53*/KRAS^{G12V}), and stable suppression of LKB1 (HBEC30KT-*shTP53*/KRAS^{G12V}/*shLKB1*).[17] **Figure 4** shows the dramatic increase of hybrid probe activation in malignant HCC4017 cells over HBEC30KT epithelial cells (see Figure S19 and S20 for the entire time course, Supporting Information). To further pinpoint which oncogenic signature is responsible for the difference in organelle acidification, the fluorescence activation pattern of hybrid nanoprobe in the isogenic progression series of HBEC30KT was imaged (Figure S21–S23, Supporting Information). To quantify the activation kinetics across different cell lines, the numbers of fluorescent dots in the red channel ($N_{6.2}$) and blue channel ($N_{5.3}$) normalized to the total number of fluorescent dots ($N_{6.9}$) were calculated as a function of time (**Figure 5**). Results demonstrate that KRAS mutation is responsible for the dramatic increase in the acidification of endocytic organelles. Our data are consistent with previous
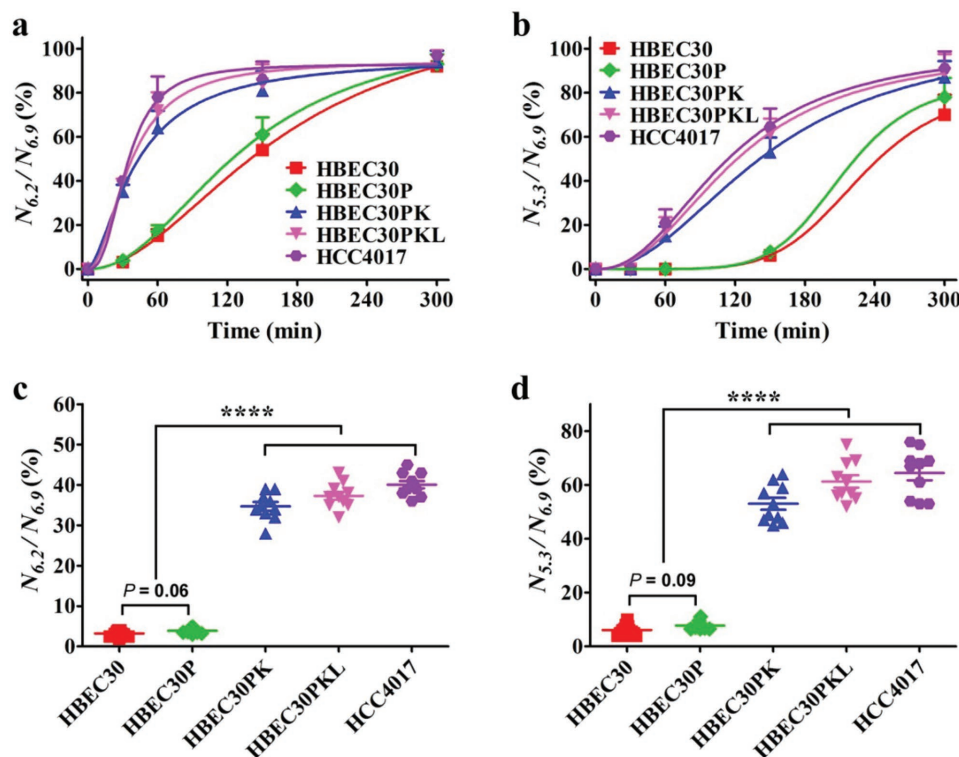
Figure 5. Kinetics of organelle acidification in an isogenic progression series of HBEC30 cells. a,b) The ratios of the number of fluorescent dots in the the red channel (a) and the blue channel (b) to the total number of fluorescent dots as a function of time pinpoint KRAS mutation instead of P53 or LKB1 suppression as the dominant driver for organelle acidification. c) The ratio of fluorescent dots in the red channel to the total number of fluorescent dots at 30 min. Ten distinct cells were imaged and calculated. Significant difference between HBEC30KT-*shTP53* and HBEC30KT-*shTP53*/KRAS^{G12V} cells was observed. d) The ratio of fluorescent dots in blue channel to the total number of fluorescent dots at 150 min. Significant difference between HBEC30KT-*shTP53* and HBEC30KT-*shTP53*/KRAS^{G12V} cells was observed. Two-way analysis of variance and Tukey's multiple comparison tests were performed to assess statistical significance of observed difference between KRAS mutated cell lines and KRAS wild-type cell lines. $n = 10$, $\alpha = 0.05$, ****$P < 0.0001$.

findings that KRAS/LKB1 mutated cells rely on lysosomal catabolism for growth and survival.[18]

In addition to the isogenic cell lines, we also quantified the acidification rates of endocytic organelles in seven additional lung cancer cell lines with different genetic background (Table S6, Figure S24–S30, Supporting Information). Using the digitization method, the number of (100), (110), and (111) organelles normalized to the total number of fluorescent dots was quantified. We observed the maturation peak of (110) dots in KRAS mutated cells by 30 min, the peak of (110) dots in KRAS wild type cells by 60 min. For the (111) dots, the half maximal maturation time was 60 min and 90 min for KRAS mutated cells and KRAS wild-type cells, respectively (**Figure 6**). Results show that the activation rates of KRAS mutated cells including HCC44, H2009, H460, and A549 were significantly faster than cells with KRAS wild type (i.e., H2882, H1991, and H1819). These data further support that mutated KRAS is responsible for the increased acidification of endocytic organelles.

Most biological signals such as pH are analog in nature, which is continuously changing in a compartmentalized space over time.[19] Conventional biosensors (e.g., small molecular pH probes) are analog sensors that offer continuous response to the changes in biological signals. Although analog sensors are capable of distinguishing fine variations in biological signals, they often suffer from low sensitivity of detection due

to lack of signal amplification and noise introduction. In this study, a 3-in-1 design together with Erbitux functionalization for synchronized delivery allows multispectral HyUPS nanoprobes to report discretized pH intervals that query multiple operator-predetermined pH transitions in the same experiment at organellar resolution in real time. Thus this new method represents a significant advance for the quantitative high-resolution discovery power required to produce new insights into the regulation of single endosome biogenesis and the coupling of organelle maturation to dynamic cell biological regulatory systems. As an important test case, these sensors, together with a binary data analytics strategy, permitted precision quantification of distinct organelle maturation rates in multiple genetic backgrounds and revealed a robust oncogenic signature in KRAS-mutant cancer cells. The accelerated acidification of catabolic organelles, detected across mutant KRAS cell lines, suggests a previously unrecognized regulatory system that can be hijacked by oncogenes to support the macropinocytosis and lysosomal catabolism of macromolecules required to satisfy aberrant nutrient demands.[17,19]

In conclusion, we report the successful development of multispectral UPS nanoprobes as a simple imaging tool to quantify the acidification rates of endocytic organelles in live cells. Incorporation of multiple fluorophore-encoded copolymers with discretized pH transitions in one nanoparticle system allowed
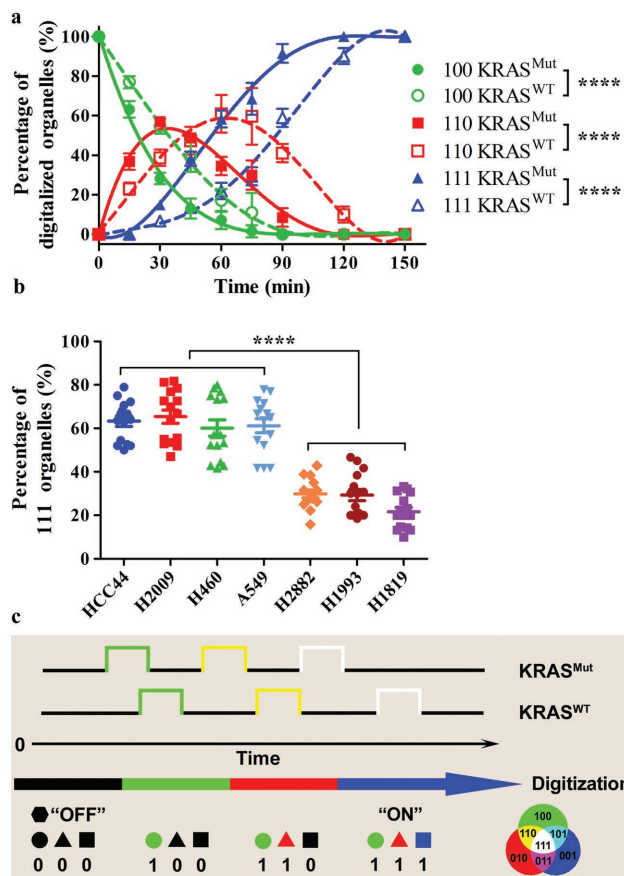
COMMUNICATION

Figure 6. Kinetics of organelle acidification among a panel of lung cancer cell lines with different genetic backgrounds. a) Percentage of pH digitized punctate showing organelle acidification in KRAS wild type and mutated cell lines. Cells were incubated with Erb-HyUPS nanoprobe at 4 °C, washed, incubated for 5 min at 37 °C, then imaged over 150 min. Ten distinct cells were imaged for each time point. b) The white dots (digital code: 111) at 75 min are normalized by the total number of dots. Significant difference between KRAS mutated cell lines and KRAS wild-type cell lines indicates that KRAS mutation is responsible for the organelle maturation. Two-way analysis of variance and Tukey's multiple comparison tests were performed to assess statistical significance of observed difference between KRAS mutated cell lines and KRAS wild-type cell lines. $n = 10$, $\alpha = 0.05$, ****$P < 0.0001$. c) Schematic illustration of the digitized signal output between KRAS wild type and mutated cells over time. KRAS mutation accelerates the acidification rates of endocytic organelles.

sequential activation and binary sensing of luminal pH at different stages of organelle maturation. Copolymerization strategy can be further implemented to establish hybrid nanoprobes with more refined, operator-predetermined control of the transition pH from 4.0 to 7.4.[20] This nanotechnology-enabled, chemical digitization paradigm offers a new imaging strategy in fundamental organelle biology studies to identify cell signaling pathways that regulate endo/lysosomal functions. In addition to cancer, this nanoplatform may also discover new biology in diseases characterized by endo/lysosomal dysfunctions, such as lysosomal storage diseases, Alzheimer's dementia, and autoimmunity.

Supporting Information

Supporting Information is available from the Wiley Online Library or from the author.

[1] a) M.-K. So, C. Xu, A. M. Loening, S. S. Gambhir, J. Rao, *Nat. Biotechnol.* **2006**, *24*, 339; b) G. Von Maltzahn, J.-H. Park, K. Y. Lin, N. Singh, C. Schwöppe, R. Mesters, W. E. Berdel, E. Ruoslahti, M. J. Sailor, S. N. Bhatia, *Nat. Mater.* **2011**, *10*, 545; c) E. G. Bellomo, M. D. Wyrsta, L. Pakstis, D. J. Pochan, T. J. Deming, *Nat. Mater.* **2004**, *3*, 244; d) C. de las Heras Alarcón, S. Pennadam, C. Alexander, *Chem. Soc. Rev.* **2005**, *34*, 276; e) M. A. C. Stuart, W. T. Huck, J. Genzer, M. Müller, C. Ober, M. Stamm, G. B. Sukhorukov, I. Szleifer, V. V. Tsukruk, M. Urban, *Nat. Mater.* **2010**, *9*, 101.

[2] a) C. A. Mirkin, R. L. Letsinger, R. C. Mucic, J. J. Storhoff, *Nature* **1996**, *382*, 607; b) R. Elghanian, J. J. Storhoff, R. C. Mucic, R. L. Letsinger, C. A. Mirkin, *Science* **1997**, *277*, 1078; c) J. J. Storhoff, R. Elghanian, R. C. Mucic, C. A. Mirkin, R. L. Letsinger, *J. Am. Chem. Soc.* **1998**, *120*, 1959.

[3] a) G. M. Whitesides, J. P. Mathias, C. T. Seto, *Science* **1991**, *254*, 1312; b) G. M. Whitesides, B. Grzybowski, *Science* **2002**, *295*, 2418; c) J.-M. Lehn, *J. Inclusion Phenom.* **1988**, *6*, 351.

[4] F. R. Maxfield, T. E. McGraw, *Nat. Rev. Mol. Cell. Biol.* **2004**, *5*, 121.

[5] a) P. Saftig, J. Klumperman, *Nat. Rev. Mol. Cell Biol.* **2009**, *10*, 623; b) C. Settembre, A. Fraldi, D. L. Medina, A. Ballabio, *Nat. Rev. Mol. Cell Biol.* **2013**, *14*, 283.

[6] A. L. Hughes, D. E. Gottschling, *Nature* **2012**, *492*, 261.

[7] a) J. H. Lee, W. H. Yu, A. Kumar, S. Lee, P. S. Mohan, C. M. Peterhoff, D. M. Wolfe, M. Martinez-Vicente, A. C. Massey, G. Sovak, Y. Uchiyama, D. Westaway, A. M. Cuervo, R. A. Nixon, *Cell* **2010**, *141*, 1146; b) A. Majumdar, D. Cruz, N. Asamoah, A. Buxbaum, I. Sohar, P. Lobel, F. R. Maxfield, *Mol. Biol. Cell.* **2007**, *18*, 1490.

[8] a) A. H. Futerman, G. van Meer, *Nat. Rev. Mol. Cell Biol.* **2004**, *5*, 554; b) F. M. Platt, B. Boland, A. C. van der Spoel, *J. Cell. Biol.* **2012**, *199*, 723.

[9] S. L. Schmid, *Annu. Rev. Biochem.* **1997**, *66*, 511.

[10] O. A. Weisz, *Int. Rev. Cytol.* **2003**, *226*, 259.

[11] J. R. Casey, S. Grinstein, J. Orlowski, *Nat. Rev. Mol. Cell Biol.* **2010**, *11*, 50.

[12] K. Zhou, Y. Wang, X. Huang, K. Luby-Phelps, B. D. Sumer, J. Gao, *Angew. Chem., Int. Ed. Engl.* **2011**, *50*, 6109.

[13] a) K. Zhou, H. Liu, S. Zhang, X. Huang, Y. Wang, G. Huang, B. D. Sumer, J. Gao, *J. Am. Chem. Soc.* **2012**, *134*, 7803;

Materials
Views

www.MaterialsViews.com

ADVANCED
MATERIALS
www.advmat.de

COMMUNICATION

b) Y. Wang, K. Zhou, G. Huang, C. Hensley, X. Huang, X. Ma, T. Zhao, B. D. Sumer, R. J. DeBerardinis, J. Gao, *Nat. Mater.* **2014**, *13*, 204.

[14] G. P. Adams, L. M. Weiner, *Nat. Biotechnol.* **2005**, *23*, 1147.

[15] a) L. Jahreiss, F. M. Menzies, D. C. Rubinsztein, *Traffic* **2008**, *9*, 574; b) Q. Zhang, Y. Li, R. W. Tsien, *Science* **2009**, *323*, 1448; c) J. P. Luzio, P. R. Pryor, N. A. Bright, *Nat. Rev. Mol. Cell Biol.* **2007**, *8*, 622.

[16] C. Commisso, S. M. Davidson, R. G. Soydaner-Azeloglu, S. J. Parker, J. J. Kamphorst, S. Hackett, E. Grabocka, M. Nofal, J. A. Drebin, C. B. Thompson, J. D. Rabinowitz, C. M. Metallo, M. G. Vander Heiden, D. Bar-Sagi, *Nature* **2013**, *497*, 633.

[17] R. D. Ramirez, S. Sheridan, L. Girard, M. Sato, Y. Kim, J. Pollack, M. Peyton, Y. Zou, J. M. Kurie, J. M. Dimaio, S. Milchgrub, A. L. Smith, R. F. Souza, L. Gilbey, X. Zhang, K. Gandia, M. B. Vaughan, W. E. Wright, A. F. Gazdar, J. W. Shay, J. D. Minna, *Cancer Res.* **2004**, *64*, 9027.

[18] H. S. Kim, S. Mendiratta, J. Kim, C. V. Pecot, J. E. Larsen, I. Zubovych, B. Y. Seo, J. Kim, B. Eskiocak, H. Chung, E. McMillan, S. Wu, J. De Brabander, K. Komurov, J. E. Toombs, S. Wei, M. Peyton, N. Williams, A. F. Gazdar, B. A. Posner, R. A. Brekken, A. K. Sood, R. J. Deberardinis, M. G. Roth, J. D. Minna, M. A. White, *Cell* **2013**, *155*, 552.

[19] J. Huotari, A. Helenius, *EMBO J.* **2011**, *30*, 3481.

[20] X. Ma, Y. Wang, T. Zhao, Y. Li, L. C. Su, Z. Wang, G. Huang, B. D. Sumer, J. Gao, *J. Am. Chem. Soc.* **2014**, *136*, 11085.